



1 **Global radiative effects of solid fuel cookstove aerosol emissions**

2 Yaoxian Huang¹, Nadine Unger², Trude Storelvmo³, Kandice Harper¹, Yiqi Zheng³, and Chris
3 Heyes⁴

4 ¹School of Forestry and Environmental Studies, Yale University, New Haven, CT 06511, USA

5 ²College of Engineering, Mathematics and Physical Sciences, University of Exeter, Exeter, EX4
6 4QE, UK

7 ³Department of Geology and Geophysics, Yale University, New Haven, CT 06511, USA

8 ⁴International Institute for Applied Systems Analysis, Laxenburg, Austria

9 *Correspondence to:* Y. Huang (yaoxian.huang@yale.edu)

10 **Abstract.** We apply the NCAR CAM5-Chem global aerosol-climate model to quantify the net
11 global radiative effects of black and organic carbon aerosols from global and Indian solid fuel
12 cookstove emissions for the year 2010. Our updated assessment accounts for the direct radiative
13 effects, changes to cloud albedo and lifetime (aerosol indirect effect, AIE), impacts on clouds via
14 the vertical temperature profile (semi-direct effect, SDE), and changes in the surface albedo of
15 snow and ice (surface albedo effect). In addition, we provide the first estimate of household solid
16 fuel black carbon emission effects on ice clouds. Anthropogenic emissions are from the IIASA
17 GAINS ECLIPSE V5a inventory. A global dataset of black carbon (BC) and organic aerosol (OA)
18 measurements from surface sites and aerosol optical depth (AOD) from AERONET is used to
19 evaluate the model skill. Compared with observations, the model successfully reproduces the
20 spatial patterns of atmospheric BC and OA concentrations, and agrees with measurements to
21 within a factor of 2. Globally, the simulated AOD agrees well with observations, with normalized
22 mean bias close to zero. However, the model tends to underestimate AOD over India and China
23 by ~ 19% but overestimate it over Africa by ~ 25%. Without BC serving as ice nuclei (IN), global
24 and Indian solid fuel cookstove aerosol emissions have a net cooling impact on global climate of
25 $-141 \pm 4 \text{ mW m}^{-2}$ and $-12 \pm 4 \text{ mW m}^{-2}$, respectively. The net radiative impacts are dominated by
26 the AIE and SDE mechanisms, which originate from enhanced cloud condensation nuclei
27 concentrations for the formation of liquid and mixed-phase clouds, and a suppression of convective
28 transport of water vapor from the lower troposphere to the upper troposphere/lower stratosphere
29 that in turn leads to reduced ice cloud formation. When BC is allowed to behave as a source of IN,



30 the net global climate impacts of the global and Indian solid fuel cookstove emissions range from
31 -260 to $+135$ mW m^{-2} and -33 to $+24$ mW m^{-2} , with globally averaged values -51 ± 210 and $0.3 \pm$
32 29 mW m^{-2} respectively. The uncertainty range is calculated from sensitivity simulations that alter
33 the maximum freezing efficiency of BC across a plausible range: 0.01, 0.05 and 0.1. BC-ice cloud
34 interactions lead to substantial increases in high cloud (< 500 hPa) fractions. Thus, the net sign of
35 the impacts of carbonaceous aerosols from solid fuel cookstoves on global climate (warming or
36 cooling) remains ambiguous until improved constraints on BC interactions with mixed-phase and
37 ice clouds are available.

38 1. Introduction

39 Worldwide 2-3 billion people rely on solid fuels for the majority of their energy needs (Legros et
40 al., 2009). This household biomass combustion includes burning wood fuel, agricultural residues
41 and dung for cooking, heating and lighting. Emissions from household solid fuel combustion
42 include greenhouse gases (carbon dioxide and methane), black carbon (BC), organic carbon (OC),
43 and other trace gases (e.g., nitrogen oxides). Globally, BC from household solid fuel emissions
44 accounts for approximately 25% of the total anthropogenic BC emissions (Bond et al., 2013).
45 Among different types of cookstoves, advanced charcoal stoves show lowest BC emission factors,
46 followed by simple charcoal, advanced biomass, rocket and simple wood stoves, respectively
47 (Garland et al., 2017). In India, residential biofuel combustion represents the dominant energy
48 sector and accounts for over 50% of the total source of BC and OC emissions (Klimont et al.,
49 2009). BC-rich household solid fuel emission plays an important role in affecting regional air
50 quality (Archer-Nicholls et al., 2016; Carter et al., 2016; Liu et al., 2016) and influencing global
51 climate change (Bauer et al., 2010; Butt et al., 2016; Venkataraman, 2005). The human health
52 consequences of solid fuel combustion are substantial (Archer-Nicholls et al., 2016; Ezzati and
53 Kammen, 2002; Lelieveld et al., 2015). Nearly 9% of the global burden of disease is attributable
54 to exposure to household air pollution from solid fuels, equivalent to 2.9 million premature deaths
55 and 86 million disability adjusted life years (DALYs) annually (GBD 2015 Risk Factors
56 Collaborators, 2016). Half of the world's population is exposed to indoor air pollution, mainly
57 attributable to solid fuel usage for household cooking and heating (Bonjour et al., 2013; Smith et
58 al., 2014).



59 Carbonaceous aerosols from solid fuel combustion interact with the Earth's radiation budget
60 directly by absorbing and scattering solar radiation (direct radiative effect, DRE) and indirectly by
61 changing cloud albedo and lifetime (aerosol indirect effect, AIE), modifying the vertical
62 temperature profile (semi-direct effect, SDE), and changing the surface albedo over snow and ice
63 (surface albedo effect, SAE) (Boucher et al., 2013; Chung, 2005; Chylek and Wong, 1995; Ghan,
64 2013; Ghan et al., 2012; Myhre et al., 2013). Carbonaceous aerosols affect cloud albedo and
65 lifetimes (the AIE) by acting as cloud condensation nuclei (CCN) or ice nuclei (IN), thus
66 modifying cloud properties and changing the top-of-atmosphere (TOA) radiative fluxes
67 (Lohmann, 2002; Lohmann et al., 2000; Penner et al., 1992; Pierce et al., 2007; Spracklen et al.,
68 2011b). The net climatic effect of carbonaceous aerosols from household solid fuel combustion is
69 not well constrained and even the sign is uncertain (Bond et al., 2013). Bauer et al. (2010)
70 estimated that the aerosol net global climate impact of residential biofuel carbonaceous aerosol
71 emissions is -130 mW m^{-2} . Kodros et al. (2015) have estimated that net DRE of solid fuel aerosol
72 emissions ranges from -20 to $+60 \text{ mW m}^{-2}$, AIE from -20 to $+10 \text{ mW m}^{-2}$, with uncertainties due to
73 assumptions of the aerosol emission masses, size distribution, aerosol optical properties and
74 mixing states. Butt et al. (2016) reported that the DRE and AIE of the residential emission sector
75 (including coal) ranged from -66 to $+21 \text{ mW m}^{-2}$, and from -52 to -16 mW m^{-2} , respectively.
76 However, neither of the latter two studies consider the aerosol cloud-lifetime effect (second
77 indirect effect), SDE and SAE. From the perspective of policy-relevant country-level assessment
78 of cookstove burning on global climate, Lacey and Henze (2015) revealed that solid fuel cookstove
79 aerosol emissions resulted in global air surface temperature changes ranging from 0.28 K cooling
80 to 0.16 K warming, concluding that emissions from China, India and Ethiopia contributed the most
81 to the global surface temperature changes (Lacey et al., 2017).

82 None of the previous assessments have included BC-ice cloud interactions that can exert a large
83 influence on the atmospheric radiation balance. A recent study by Kulkarni et al. (2016) showed
84 that BC could act as IN, which was also shown by past lab and field findings (Cozic et al., 2008;
85 DeMott et al., 1999; Koehler et al., 2009). With BC as IN, Penner et al. (2009) estimated that the
86 total radiative forcing of anthropogenic and biomass BC emissions was -300 to -400 mW m^{-2} , with
87 IN parameterizations following Liu and Penner (2005) and Kärcher et al. (2006). Gettelman et al.
88 (2012) further concluded that AIE from BC emissions was -60 mW m^{-2} , with IN parameterization
89 following Barahona and Nenes (2009). Hence, a re-assessment of the global climate change



90 impacts of carbonaceous aerosol emissions from the solid fuel cookstove sector that newly
91 incorporates BC as IN is urgently needed.

92 Here, we employ a global aerosol-climate model to quantify the impacts of solid fuel cookstove
93 carbonaceous aerosol emissions globally and from India on global climate change. Sect. 2 presents
94 the Methods including the evaluation measurement data sets for BC, OA and aerosol optical depth
95 (AOD), the model description and experimental design. Sect. 3 details the results of the model
96 evaluation and the impacts of the global and Indian solid fuel cookstove emissions on the
97 atmospheric radiation budget and global climate. Discussion and summary are provided in Sect.
98 4.

99 2. Methods

100

101 2.1 BC and OC evaluation measurement database

102 Ground-based BC observations are from IMPROVE (the Interagency Monitoring of PROtected
103 Visual Environment, <http://vista.cira.colostate.edu/Improve/>) for the year 2010 over North
104 America (Malm et al., 1994), EMEP (the European Monitoring and Evaluation Programme,
105 <http://ebas.nilu.no>) for 2009-2013 over Europe, and sporadic measurement campaigns for China
106 and India. Elemental carbon (EC) concentrations are measured using Thermal Optical Reflectance
107 (TOR) (Chow et al., 1993, 2004; EMEP/MSC-W et al., 2014). Our measurement database
108 comprises a total of 152 sites from IMPROVE, 28 sites from EMEP, 35 sites for China, and 41
109 sites for India. The number of urban sites includes 8 from IMPROVE, 5 from EMEP, 17 for China,
110 and 23 for India.

111 A global network of aerosol mass spectrometer (AMS) surface measurements for organic aerosol
112 (OA) for 2000-2008 are used to compare with model simulations (Spracklen et al., 2011a; Zhang
113 et al., 2007; Zheng et al., 2015). The AMS technique measures hydrocarbon-like OA (HOA),
114 oxygenated OA (OOA) and total OA (HOA + OOA). HOA is a surrogate for primary OA (POA)
115 emitted directly from fossil fuel and biomass burning, while OOA is a surrogate for secondary OA
116 (SOA). In this study, we compare monthly mean total OA with model simulated total OA (POA +
117 SOA). The majority of the AMS measurements in the surface concentration database were made
118 prior to 2005.



119 Ground-based AOD observations from AERONET (AErosol RObtic NETwork,
120 <https://aeronet.gsfc.nasa.gov>) during 1993-2016 are applied to examine model skill (Dubovik and
121 King, 2000; Holben et al., 1998, 2001). A climatological AOD value averaged over 1993-2016 for
122 each site is used to compare with the model simulation. The AERONET version 2 level-2 product
123 is used in this study.

124 **2.2 NCAR CAM5-Chem global model description**

125 We apply the NCAR Community Atmosphere Model version 5.3 with chemistry (CAM5-Chem)
126 within the Community Earth System Model (CESM) version 1.2.2 (Emmons et al., 2010;
127 Lamarque et al., 2012; Tilmes et al., 2015). The oxidant-aerosol system is fully coupled in CAM5-
128 Chem. The horizontal resolution of CAM5-chem is 0.9° latitude by 1.25° longitude, with 56
129 vertical levels from surface up to about 40 km. In the standard CAM5-Chem, aerosol
130 microphysical processes are represented using a 3-mode scheme (MAM3; aitken, accumulation
131 and coarse modes). MAM3 simulates both mass and number concentrations of aerosols. Aerosol
132 size distributions in each mode are assumed to be lognormal (Liu et al., 2012). The model treats
133 the effects of aerosol acting as CCN in liquid-phase clouds (Ghan et al., 2012). The aerosol
134 components in MAM3 include BC, primary organic matter (POM), secondary organic aerosol
135 (SOA), sulfate, sea salt and dust, which are assumed to be internally mixed within each lognormal
136 mode. Mass yields of semi-volatile organic gas-phase species (SOAG) from emissions of isoprene,
137 monoterpenes, big alkanes and alkenes, as well as toluene are prescribed (Emmons et al., 2010;
138 Liu et al., 2012; Tilmes et al., 2015). The condensable SOAG reversibly and kinetically partitions
139 into the aerosol phase to form SOA in CAM5-Chem as described in Liu et al. (2012).

140 **2.3 Emissions**

141 Global anthropogenic emissions are from the IIASA (International Institute for Applied System
142 Analysis) Greenhouse Gas-Air Pollution Interactions and Synergies (GAINS) integrated
143 assessment model ECLIPSE V5a (Evaluating the Climate and Air Quality Impacts of Short-lived
144 Pollutants version 5a) for the year 2010 (Amann et al., 2011, 2013; Klimont et al., 2017; Stohl et
145 al., 2015). Species in ECLIPSE V5a include BC, POM, sulfur dioxide, nitrogen oxides, carbon
146 monoxide, volatile organic compounds, and ammonium, with their annual global budgets for the
147 year 2010 shown in Table 1. ECLIPSE V5a emissions available at 0.5° latitude by 0.5° longitude



148 spatial resolutions are re-gridded to the model spatial resolution. ECLIPSE V5a does not include
149 shipping or wildfire biomass burning emissions, which are instead obtained from the IPCC AR5
150 RCP8.5 scenario for the year 2010 (Riahi et al., 2011).

151 **2.4 Simulations**

152 Atmosphere-only simulations are performed in specified dynamics (SD) mode with offline
153 meteorological fields from the Goddard Earth Observing System model version 5 (GEOS-5). In
154 this SD mode configuration, the internally derived meteorological fields (e.g., horizontal wind
155 component, air temperature and latent heat flux) are nudged by 10% towards reanalysis fields from
156 GEOS-5 for every model time step. The nudging technique in CAM5-Chem has been evaluated to
157 quantify the aerosol indirect effect in order to reduce the influence of natural variability
158 (Kooperman et al., 2012). Sea surface temperature and sea ice in the model are prescribed from
159 the Climatological/Slab-Ocean Data Model (DOCN) and Climatological Ice Model (DICE)
160 respectively, with monthly-varying decadal mean averaged over 1981-2010.

161 We perform three sets of model simulations using the model configurations shown in Table 2. The
162 first set of simulations represents the control with anthropogenic emissions following ECLIPSE
163 V5a, as described above (hereafter referred to as BASE). The second set of simulations are
164 identical to the BASE simulation except the global solid fuel cookstove emissions for aerosols and
165 gas-phase aerosol and ozone precursors are set to zero (termed as GBLSF_OFF). The third set of
166 simulations is identical to BASE except the solid fuel cookstove emissions are set to zero over the
167 Indian sub-continent (termed as INDSF_OFF). We run all the above simulations for 6 years from
168 2005 to 2010, with the first year discarded as spin-up and the last five years averaged for output
169 analysis. The differences between BASE and GBLSF_OFF isolate the impacts of the global solid
170 fuel cookstove sector aerosol emissions, and the differences between BASE and INDSF_OFF
171 isolate the impacts of the Indian solid fuel cookstove sector aerosol emissions. Top-of-the-
172 atmosphere (TOA) aerosol shortwave (SW) and longwave (LW) radiative effects are calculated
173 using the Rapid Radiative Transfer Model for GCMs (RRTMG) that is coupled to CAM5-Chem
174 (Ghan, 2013; Ghan et al., 2012).

175 **3 Results**

176 **3.1 Evaluation of surface BC and OA concentrations**



177 Surface observation networks from IMPROVE, EMEP, and various campaigns in China and India
178 are employed to compare with model simulations, as shown in Figure 1. We diagnose the
179 normalized mean bias (NMB) for each source region, calculated as

$$180 \quad \text{NMB} = \left(\frac{\sum_i (M_i - O_i)}{\sum_i O_i} \right) \times 100\% \quad (1)$$

181 where M and O represent monthly mean model simulated and observational concentrations at site
182 i respectively, and \sum is the sum over all the sites within a source region.

183 In general, the model simulated surface BC concentrations agree with observations to within a
184 factor of 2, consistent with previous studies (Huang et al., 2013; Wang et al., 2011, 2014a, 2014b).
185 A total of 41 surface BC observational sites are used to evaluate the model simulation over India
186 (Fig. 1a). On average, the model underestimates surface BC concentrations by approximately 45%
187 and 34% over urban and rural sites respectively, with a total NMB -41% (Fig. 1a), which implies
188 a marked underestimation of the BC emissions in India. Previous modeling studies have also
189 reported large underestimates of BC surface concentrations over India against observations
190 (Gadhavi et al., 2015; He et al., 2014; Zhang et al., 2015). Part of the model/measurement
191 discrepancy is related to a sampling bias because the majority of the observations are located over
192 urban or heavily polluted regions. For China sites, the NMB value is -16% (Fig. 1b). Similar to
193 India, the model substantially underestimates the surface BC concentrations over urban sites with
194 a NMB of -30%. However, the model performs relatively well over rural areas, with a NMB close
195 to zero. For IMPROVE, the NMB values for rural and urban sites are -15% and -43%, respectively,
196 with a total NMB -28% (Fig. 1c). Over Europe, the model simulated surface BC concentrations
197 agree quite well with observations, with a NMB value of -8%, although two urban sites show
198 substantial model underestimation (Fig. 1d).

199 The 40 AMS surface OA measurements are grouped into three categories: East Asia (8 sites),
200 North America (17 sites) and Europe (15 sites) (Spracklen et al., 2011a; Zhang et al., 2007; Zheng
201 et al., 2015). Figure 2 shows the evaluation of simulated surface OA against observations. Over
202 East Asia, the model slightly underestimates observed OA, with a NMB of -8.5% (Fig. 2a). In
203 contrast, the simulated OA concentrations overestimate the measurements by over a factor of 2 in
204 North America, with a NMB value of 124% (Fig. 2b). For the European sites, we find a simulated



205 OA overestimation of measured concentrations by up to $0.9 \mu\text{g m}^{-3}$, corresponding to a NMB of
206 +32% (Fig. 2c).

207 3.2 Evaluation of model AOD

208 Figure 3 compares simulated AOD values against observations over nine regions across the globe,
209 including India, China, Rest of Asia (excluding China and India), Africa, South America, North
210 America, Europe, Australia and remote regions. Over India, the simulated annual mean AOD is
211 lower than observations by about 16% (Fig. 3a), with large bias sources mainly from the northern
212 India regions (e.g., New Delhi and Kanpur). This is consistent with Quennehen et al. (2016) who
213 also reported that model simulated AOD values were generally lower than satellite-derived AOD
214 over northern India, using the same emission inventory as our study. As discussed in Sect. 3.1,
215 model simulated surface BC concentrations over India are also underestimated (by up to 41%),
216 therefore, the low bias of model simulated AOD can be attributed, in part, to the underestimation
217 of Indian BC emissions from ECLIPSE V5a emission inventory (Stohl et al., 2015), although
218 global anthropogenic BC budgets in ECLIPSE V5a lie in the high end compared with previous
219 studies (Bond et al., 2004, 2013; Janssens-Maenhout et al., 2015). A similar pattern is found over
220 China (Fig. 3b) and the rest of Asia (Fig. 3c), with NMB values of -21% and -15% respectively.
221 Model simulated AOD values from several sites in West Asia (Fig. 3c) are higher than
222 observations, which is probably caused by the model overestimation of dust emissions (He and
223 Zhang, 2014). This directly leads to annual mean model simulated AOD values over Africa 25%
224 higher than observations because Saharan dust emissions dominate the AOD over North Africa
225 (Fig. 3d). For South America, the model generally agrees quite well with observations (Fig. 3e),
226 except for a few sites where model simulated AOD values are lower than observations by more
227 than a factor of 2. This is probably due to the model underestimation of biomass burning emissions
228 there (Reddington et al., 2016). AOD values over North America (Fig. 3f) and Europe (Fig. 3g)
229 are relatively lower (with values generally < 0.3), due to lower anthropogenic emissions. In these
230 two regions, modeled AOD agrees with observations within a factor of 2, with NMB values -20%
231 and -18% respectively. CAM5-Chem overestimates AOD over Australia (Fig. 3h) and remote sites
232 (Fig. 3i), with NMB values of +69% and +47%, respectively. Globally, model simulated AOD
233 agrees quite well with observations, with NMB values close to zero.

234 3.3 Contribution of solid fuel cookstove sector emissions to atmospheric BC and POM



235 3.3.1 BC

236 Annual BC emissions and budgets are reported in Table 3 based on the anthropogenic inventory
237 from ECLIPSE V5a. Annual BC emissions from the global and Indian solid fuel cookstove
238 emissions are 2.31 and 0.36 Tg yr⁻¹, accounting for 23.7% and 3.7% of the total BC emissions. For
239 the control simulation, global annual mean BC burden and lifetime are 0.12 Tg and 4.5 days,
240 respectively (Table 3), at the low end of the range estimated by AeroCom (Schulz et al., 2006;
241 Textor et al., 2006).

242 Figure 4 shows the zonal mean BC concentrations from the control simulation (Fig. 4a), global
243 (Fig. 4b) and Indian (Fig. 4c) solid fuel cookstove emissions respectively. For the control
244 simulation, in general, the highest BC concentrations (by up to 0.40 µg m⁻³) occur at the surface
245 over the emission source regions in the mid-latitudes (e.g., China and India). In the tropics and
246 mid-latitudes, zonal mean BC concentrations decrease with increasing altitude, due to wet removal
247 and deposition, as found in Huang et al. (2013). A similar vertical distribution is observed for the
248 impacts from global and Indian solid fuel cookstove emissions, although the magnitude is smaller,
249 compared with the control simulation. Annual mean BC burdens from global and Indian solid fuel
250 cookstove emissions account for about 24% and 5% of that in the control simulation (0.12 Tg).

251 3.3.2 POM

252 Global POM emissions are mainly from biomass burning (31 Tg yr⁻¹) and anthropogenic emissions
253 (18.9 Tg yr⁻¹), with global and Indian solid fuel cookstove emissions accounting for, 21% and
254 3.4% respectively, of the total POM emissions (Table 3). In our control simulation, the annual
255 mean POM burden is 0.66 Tg, and the global annual mean POM lifetime is 4.8 days (Table 3).

256 In Figure 5, we show the annual zonal mean POM concentrations for the control simulation (Fig.
257 5a) and for global (Fig. 5b) and Indian (Fig. 5c) solid fuel cookstove emissions. There are two
258 maxima in the annual zonal mean POM concentrations near the surface. One is located in the
259 tropics due to the large biomass burning emissions there, and the other is located over mid-latitude
260 regions and originates mainly from anthropogenic emissions (Chung and Seinfeld, 2002; Huang
261 et al., 2013). For POM concentrations from global solid fuel cookstove emissions, a single
262 maximum is evident in the Northern Hemisphere (NH) subtropics at the surface (Fig. 5b). The



263 surface maximum for the Indian solid fuel cookstove emissions reaches a maximum in the NH
264 subtropics. The annual mean POM burdens from global and Indian solid fuel cookstove emissions
265 are 0.13 Tg and 0.027 Tg respectively.

266 **3.4 Impacts of solid fuel cookstove aerosol emissions on global climate change**

267

268 **3.4.1 Direct radiative effect (DRE)**

269 The DRE impacts of the global and Indian solid fuel cookstove emissions are shown in Figure 6.
270 For the global solid fuel cookstove sector, the globally averaged DRE from aerosol emissions is
271 $+70 \pm 3 \text{ mW m}^{-2}$ without treating BC as IN, which is a warming effect. The positive DRE from
272 global solid fuel cookstove emissions shows large spatial variability, with the largest impacts
273 located over western Africa, followed by India and China (figure not shown). The contributions of
274 BC and POM to DRE are $+105 \pm 4$ (warming) and -14 ± 1 (cooling) mW m^{-2} , respectively. In other
275 words, the warming effect of BC is partially offset by the cooling effect from POM. Additional
276 cooling effects may come from sulfate and SOA. CAM5-Chem assumes that BC is internally
277 mixed with other components in the accumulation mode and simulates enhanced absorption when
278 BC is coated by soluble aerosol components and water vapor (Ghan et al., 2012), which results in
279 larger estimates of the DRE from BC (Bond et al., 2013; Jacobson, 2001b).

280 The DRE from Indian solid fuel cookstove emissions also corresponds to a net warming effect
281 (Fig. 6), with a global annual mean value of $+11 \pm 1 \text{ mW m}^{-2}$. Large impacts are found over
282 continental India, the Tibetan Plateau and southeastern China. On a global annual basis, DRE
283 values from BC and POM emissions from the Indian solid fuel cookstove sector are $+18 \pm 1$ and
284 $-3 \pm 0.2 \text{ mW m}^{-2}$, respectively.

285 **3.4.2 Aerosol indirect, semi-direct and surface albedo effects: BC not active as IN**

286 Global annual mean AIE and SAE values from global and Indian solid fuel cookstove aerosol
287 emissions are shown in Figure 6. In our study, AIE includes the first (albedo) and second (lifetime)
288 indirect effects, as well as the semi-direct effect. Annually averaged AIE from the global solid fuel
289 cookstove sector is $-226 \pm 5 \text{ mW m}^{-2}$ (Fig. 6), with annual mean shortwave (SW) AIE -122 ± 22
290 mW m^{-2} and longwave (LW) AIE $-104 \pm 17 \text{ mW m}^{-2}$, without treating BC as IN. Both the annual
291 mean SW and LW AIE thus yield cooling effects. The cooling signals of SW AIE mainly occur



292 over the western coast of South America, west and east coasts of Africa, South China and Himalaya
293 regions (figure not shown). This is directly linked to the contribution of global solid fuel cookstove
294 aerosol emissions to CCN (Pierce et al., 2007), which increases the cloud droplet number
295 concentrations (CDNC) and cloud liquid water path (CLWP). Figure 7 shows the global vertically-
296 integrated distribution of CLWP from the contribution of global solid fuel cookstove aerosol
297 emissions. The higher CLWP is due to the enhanced lifetime of liquid and mixed-phase clouds,
298 which therefore reflect more solar radiation, leading to cooling effect. For the LW AIE, the largest
299 cooling effect is found over tropical regions, especially over southern India and the Indian Ocean.
300 In order to investigate the causes of the LW AIE cooling effect, we analyze the cloud fraction
301 change over a defined region (Latitude:0-20°N; Longitude:60-90°E) due to the effect from the
302 global solid fuel cookstove sector. As shown in Figure 8a, cloud fraction in the lower troposphere
303 increases. However, in the middle and upper troposphere cloud fraction decreases by up to 0.6%,
304 with the strongest decrease found at ~150 hPa. We further analyze the changes in shallow and deep
305 convective mass fluxes of moisture over the same domain. As shown in Figure 8b, moist shallow
306 convective mass flux generally shows increases in the lower troposphere, which means that solid
307 fuel cookstove aerosol emissions enhance the convective transport of water vapor within the
308 boundary layer. By contrast, the deep convective mass flux demonstrates decreases from surface
309 up to the middle troposphere (Fig. 8c). This indicates that solid fuel cookstove aerosol emissions
310 may stabilize the boundary layer and inhibit the transport of water vapor from the surface to the
311 upper troposphere/lower stratosphere, which leads to decreases in ice cloud formation, thus
312 reducing cloud cover in the upper troposphere and lower stratosphere (UTLS) region at around
313 200 hPa (Fig. 8a) and a LW AIE cooling effect.

314 The global annual mean AIE from Indian solid fuel cookstove aerosol emissions accounts for
315 approximately 10% ($-22 \pm 3 \text{ mW m}^{-2}$) relative to the value of AIE from the global solid fuel
316 cookstove sector (Fig. 6), with globally averaged SW and LW AIE values of -3 ± 11 and -19 ± 11
317 mW m^{-2} respectively.

318 Global annual mean SAE values from global and Indian solid fuel cookstove sector are relatively
319 small: $+15 \pm 3$ and $-2 \pm 3 \text{ mW m}^{-2}$, respectively (Fig. 6). The warming effect is mainly due to the
320 deposition of BC on the surface of snow and sea ice (Flanner et al., 2007; Ghan, 2013; Ghan et al.,
321 2012).



322 3.4.3 Total radiative effect: BC not active as IN

323 The net total radiative effect of global and Indian solid fuel cookstove aerosol emissions are both
324 cooling, with the global annual mean estimated to be -141 ± 4 and -12 ± 4 mW m^{-2} respectively
325 (Fig. 6). This suggests that if we remove solid fuel cookstove aerosol emissions, it will result in
326 warming and thus slightly increased global surface air temperature. That being said, this is likely
327 to be quite sensitive to model representation of aerosol mixing state (Fierce et al., 2017).

328 3.4.4 Total radiative effect: BC active as IN

329 In default CAM5-Chem, BC is not treated as IN (Liu et al., 2012; Tilmes et al., 2015). However,
330 several lab and field studies have shown that BC particles could act as IN (Cozic et al., 2008;
331 DeMott et al., 1999; Koehler et al., 2009; Kulkarni et al., 2016), as discussed in Section 1.
332 Therefore, we conduct sensitivity studies in our model simulations by treating BC as an effective
333 IN, with the ice nucleation scheme by Barahona and Nenes (2008, 2009). We run three additional
334 model simulations, with model configurations identical to those in Table 2, except for the treatment
335 of BC particles as effective IN. In addition, for each model simulation, we alter the plausible
336 maximum freezing efficiency (MFE) of BC as 0.01, 0.05 and 0.1, from which the uncertainty
337 ranges of the climatic impacts from global and Indian solid fuel cookstove aerosol emissions with
338 BC as IN are quantified.

339 For the radiative effect of global solid fuel cookstove emissions with BC as IN, global annual mean
340 DRE is 99 ± 12 mW m^{-2} , ranging from $+85$ to $+107$ mW m^{-2} , which is 21-53% higher than the
341 DRE values from the default scheme (Fig. 6). Intriguingly, large globally averaged negative SW
342 AIE (-1.33 ± 0.63 W m^{-2}) and positive LW AIE ($+1.17 \pm 0.44$ W m^{-2}) for global solid fuel
343 cookstove aerosol emissions are found, with annual mean values for the SW AIE ranging from -
344 1.80 to -0.62 W m^{-2} and from $+0.66$ to $+1.44$ W m^{-2} for the LW AIE. This results in a rather
345 uncertain net AIE, with a global annual mean AIE of -163 ± 216 mW m^{-2} (Fig. 6). The reason for
346 the large global annual average negative SW AIE and positive LW AIE is a substantial increase in
347 high cloud (< 500 hPa) fractions when BC acts as an efficient IN. For instance, with $\text{MFE} = 0.1$,
348 large increases (by up to 9%) in high cloud fractions from global solid fuel cookstove aerosol
349 emissions are found over subtropical regions, especially over the southern Atlantic Ocean (Fig. 9).
350 With BC particles active as IN, ice particle sizes become smaller, leading to a slower settling



351 velocity for ice particles and thus an increase in the lifetime of ice clouds. Increases in high clouds
352 not only reflect more solar radiation back to space, but also trap more LW radiation within the
353 troposphere. For SAE, the global annual mean value is $+14 \pm 8 \text{ mW m}^{-2}$ (Fig. 6). As a result, the
354 net total radiative effect of global solid fuel cookstove aerosol emissions ranges from -260 to +
355 135 mW m^{-2} , with a global annual mean of $-51 \pm 210 \text{ mW m}^{-2}$ (Fig. 6). Again, the source of the
356 large uncertainty of the total radiative effect is due to the choice of MFE values. With $\text{MFE} = 0.01$,
357 the global mean LW AIE ($+660 \text{ mW m}^{-2}$) outweighs SW AIE (-620 mW m^{-2}), and therefore results
358 in a net warming effect. For other MFE values (0.05 and 0.1), the absolute global annual mean SW
359 AIE values are always higher than the LW AIE, leading to a net negative (i.e., cooling) total
360 radiative effect.

361 For the Indian solid fuel cookstove sector, the global annual mean net total radiative effect is 0.3
362 $\pm 29 \text{ mW m}^{-2}$, with an AIE of -18 ± 37 and a SAE of $+1 \pm 8 \text{ mW m}^{-2}$, respectively.

363 **4 Discussion and Summary**

364 In this study, we employ the atmospheric component of a global 3-D climate model CESM v1.2.2,
365 CAM5.3-Chem, to investigate the impacts of solid fuel cookstove emissions on global climate
366 change. We update the default anthropogenic emission inventory using IIASA ECLIPSE V5a for
367 the year 2010. We focus our analysis on the radiative effects of global and Indian solid fuel
368 cookstove aerosol emissions. Model performance is evaluated against a global dataset of BC and
369 OA measurements from surface sites and AOD from AERONET. Compared with observations,
370 the model successfully reproduces the spatial patterns of atmospheric BC and OA concentrations,
371 and generally agrees with measurements to within a factor of 2. Globally, the simulated AOD
372 agrees quite well with observations, with NMB values close to zero. Nevertheless, the model tends
373 to underestimate AOD values over source regions (except for Africa) and overestimate AOD over
374 remote regions. The underestimates of AOD over India and China indicate that anthropogenic
375 emissions of carbonaceous aerosols and sulfate precursors in ECLIPSE V5a are underestimated
376 because carbonaceous aerosols and sulfate account for over 60% of the AOD over these two
377 countries (Lu et al., 2011; Streets et al., 2009), which may introduce uncertainties for our climate
378 estimates. In the control simulation, the global annual mean BC burden and lifetime are 0.12 Tg
379 and 4.5 days. For POM, the burden and lifetime are 0.66 Tg and 4.8 days. Annual mean surface



380 BC (POM) concentrations over Northern India, East China and sub-Saharan Africa are 1.4, 0.74
381 and $0.11 \mu\text{g m}^{-3}$ (6.5 , 3.8 and $0.5 \mu\text{g m}^{-3}$), respectively. BC and POM burdens from global solid
382 fuel cookstove emissions are 0.026 and 0.12 Tg , while contributions from the Indian sector are
383 0.005 and 0.024 Tg , respectively.

384 In the default CESM simulations without treating BC as IN, globally averaged DRE values from
385 global and Indian solid fuel cookstove emissions are $+70 \pm 3$ and $+11 \pm 1 \text{ mW m}^{-2}$, respectively.
386 The contributions of BC and POM from global solid fuel cookstove emissions to the DRE are
387 $+105 \pm 4$ and $-14 \pm 1 \text{ mW m}^{-2}$. Global annual mean SW and LW AIE values from global solid fuel
388 cookstove emissions are -122 ± 22 and $-104 \pm 17 \text{ mW m}^{-2}$, with contributions from India yielding
389 $-3 \pm 11 \text{ mW m}^{-2}$ for the SW AIE and $-19 \pm 11 \text{ mW m}^{-2}$ for the LW AIE, respectively. The cooling
390 effect of the SW AIE is associated with the increases of CCN and CDNC, whereas the negative
391 effects of LW AIE are caused by the suppression of convection that transports water vapor from
392 lower troposphere to upper troposphere/stratosphere, thus reducing ice cloud cover. The CAM5-
393 Chem also computes the SAE, with global and Indian solid fuel cookstove emissions contributing
394 $+15 \pm 3$ and $-2 \pm 3 \text{ mW m}^{-2}$, respectively. As a result, the net total radiative effects of global and
395 Indian solid fuel cookstove emissions are -141 ± 4 and $-12 \pm 4 \text{ mW m}^{-2}$, respectively, both
396 producing a net cooling effect.

397 Sensitivity studies are carried out to examine the impacts of global and Indian solid fuel cookstove
398 emissions on climate by treating BC as an effective IN, with MFE as 0.01 , 0.05 and 0.1 ,
399 respectively. For the climate impacts of global solid fuel cookstove emissions, global annual mean
400 DRE is $+99 \pm 12 \text{ mW m}^{-2}$, which is $\sim 40\%$ higher than the default model scheme in which BC
401 particles are not treated as IN (Fig. 6). This is driven by the increases of BC burden (due to
402 prolonged BC lifetimes) from global solid fuel cookstove emissions by up to 17% with BC as IN.
403 Because the BC absorption effect dominates the DRE, increases in BC burden enhance the
404 magnitude of annual mean DRE (Jacobson, 2001a). Compared with the default model scheme,
405 significant changes in globally averaged SW AIE are found, with a global annual mean of $-1.33 \pm$
406 0.63 W m^{-2} , which is about an order of magnitude higher than that from the default scheme.
407 Moreover, in contrast to the cooling effect found in the default scheme, annual mean positive LW
408 AIE is simulated here ($+1.17 \pm 0.44 \text{ W m}^{-2}$). The above changes in cookstove emission induced
409 SW and LW AIE are caused by the substantial increases in high cloud ($< 500 \text{ hPa}$) fractions with



410 BC particles acting as IN by up to 9% due to the effect of solid fuel cookstove emissions. Large
411 increases in high cloud fractions are found mainly over tropical regions, especially over southern
412 Africa. For the SAE, similar to the model default scheme, the global annual mean value is $+14 \pm$
413 8 mW m^{-2} . Summing up the DRE, the AIE and the SAE, the net total radiative effect of global
414 solid fuel cookstove emissions is $-51 \pm 210 \text{ mW m}^{-2}$. For the Indian sector, the global mean total
415 radiative effect is $0.3 \pm 29 \text{ mW m}^{-2}$, with a net AIE -18 ± 37 and a SAE $+1 \pm 8 \text{ mW m}^{-2}$,
416 respectively.

417 We compare our simulation results with previous studies as shown in Figure 10. The globally
418 averaged DRE in our control simulation is more than four times higher than that from the baseline
419 simulation of Kodros et al. (2015), which assumes homogeneous particle mixing state (Fig. 10).
420 Annual emissions of BC from global solid fuel cookstove sector in our study (2.3 Tg C yr^{-1}) is
421 approximately 44% higher than that from global biofuel emissions (1.6 Tg C yr^{-1}) in Kodros et al.
422 (2015), which, to some extent, leads to differences in annual mean DRE values together with
423 different optical calculations. The annual mean DRE value from another study by Butt et al. (2016)
424 differs from ours in magnitude and sign, and concluded that annually averaged DRE from
425 residential combustion sources was -5 mW m^{-2} (Fig. 10). The negative effect of DRE in Butt et al.
426 (2016) is partially driven by the inclusion of SO_2 emissions ($8.9 \text{ Tg SO}_2 \text{ yr}^{-1}$) from commercial
427 coal combustion in the residential sector, leading to the cooling effect of sulfate and organic
428 aerosols outweighing the warming from BC. For AIE, our control simulation is 38 times higher
429 than that from Kodros et al. (2015) and over an order of magnitude higher than that from Butt et
430 al. (2016). Both Kodros et al. (2015) and Butt et al. (2016) used offline radiative models to
431 calculate AIE and only considered the first (albedo) aerosol indirect effect, which may partially
432 explain the AIE differences. As mentioned earlier, the AIE in our study includes aerosol first and
433 second indirect effects as well as the semi-direct effect. Lacey and Henze (2015) estimated that
434 the global surface air temperature changes due to solid wood fuel removal ranged from -0.28 K
435 (cooling) to $+0.16 \text{ K}$ (warming), with a central estimate of -0.06 K (cooling). This cooling estimate
436 is opposite to our study. However, we acknowledge that there are fundamental differences in
437 calculating the radiative effect between our study and Lacey and Henze (2015), which employed
438 absolute regional temperature potentials to quantify the climate responses.



439 Cookstove intervention programs have been implemented in developing countries, such as China,
440 India and some African countries, to improve air quality and human health and to mitigate climate
441 change (Anenberg et al., 2017; Aung et al., 2016; Carter et al., 2016). Our results suggest that
442 large-scale efforts to replace inefficient cookstoves in developing countries with advanced
443 technologies is not likely to reduce global warming through aerosol reductions, and may even lead
444 to increased global warming when aerosol-cloud interactions are taken into account. Therefore,
445 without improved constraints on BC interactions with clouds, especially mixed-phase and ice
446 clouds, the net sign of the impacts of carbonaceous aerosols from solid fuel cookstoves on global
447 climate (warming or cooling) remains ambiguous.

448 **Acknowledgements**

449 This article was developed under Assistance Agreement No. R835421 awarded by the U.S.
450 Environmental Protection Agency to SEI. It has not been formally reviewed by EPA. The views
451 expressed in this document are solely those of the authors and do not necessarily reflect those of
452 the Agency. EPA does not endorse any products or commercial services mentioned in this
453 publication. N. Unger acknowledges support from the University of Exeter, UK. We are thankful
454 for helpful discussions with S. Tilmes and S. Ghan. This project was supported in part by the
455 facilities and staff of the Yale University High Performance Computing Center.

456 **References**

- 457 Amann, M., Bertok, I., Borken-Kleefeld, J., Cofala, J., Heyes, C., Höglund-Isaksson, L.,
458 Klimont, Z., Nguyen, B., Posch, M., Rafaj, P., Sandler, R., Schöpp, W., Wagner, F. and
459 Winiwarter, W.: Cost-effective control of air quality and greenhouse gases in Europe: Modeling
460 and policy applications, *Environ. Model. Softw.*, 26(12), 1489–1501,
461 doi:10.1016/j.envsoft.2011.07.012, 2011.
- 462 Amann, M., Klimont, Z. and Wagner, F.: Regional and Global Emissions of Air Pollutants:
463 Recent Trends and Future Scenarios, *Annu. Rev. Environ. Resour.*, 38(1), 31–55,
464 doi:10.1146/annurev-environ-052912-173303, 2013.
- 465 Anenberg, S. C., Henze, D. K., Lacey, F., Irfan, A., Kinney, P., Kleiman, G. and Pillarisetti, A.:
466 Air pollution-related health and climate benefits of clean cookstove programs in Mozambique,



- 467 Environ. Res. Lett., 12(2), 25006, doi:10.1088/1748-9326/aa5557, 2017.
- 468 Archer-Nicholls, S., Carter, E., Kumar, R., Xiao, Q., Liu, Y., Frostad, J., Forouzanfar, M. H.,
469 Cohen, A., Brauer, M., Baumgartner, J. and Wiedinmyer, C.: The regional impacts of cooking
470 and heating emissions on ambient air quality and disease burden in China, Environ. Sci.
471 Technol., 50(17), 9416–9423, doi:10.1021/acs.est.6b02533, 2016.
- 472 Aung, T. W., Jain, G., Sethuraman, K., Baumgartner, J., Reynolds, C., Grieshop, A. P., Marshall,
473 J. D. and Brauer, M.: Health and Climate-Relevant Pollutant Concentrations from a Carbon-
474 Finance Approved Cookstove Intervention in Rural India, Environ. Sci. Technol., 50(13), 7228–
475 7238, doi:10.1021/acs.est.5b06208, 2016.
- 476 Barahona, D. and Nenes, A.: Parameterization of cirrus cloud formation in large-scale models:
477 Homogeneous nucleation, J. Geophys. Res. Atmos., 113(11), 1–15, doi:10.1029/2007JD009355,
478 2008.
- 479 Barahona, D. and Nenes, A.: Parameterizing the competition between homogeneous and
480 heterogeneous freezing in ice cloud formation – polydisperse ice nuclei, Atmos. Chem. Phys., 9,
481 5933–5948, doi:10.5194/acpd-9-10957-2009, 2009.
- 482 Bauer, S. E., Menon, S., Koch, D., Bond, T. C. and Tsigaridis, K.: A global modeling study on
483 carbonaceous aerosol microphysical characteristics and radiative effects, Atmos. Chem. Phys.,
484 10(15), 7439–7456, doi:10.5194/acp-10-7439-2010, 2010.
- 485 Bond, T., Venkataraman, C. and Masera, O.: Global atmospheric impacts of residential fuels,
486 Energy Sustain. Dev., 8(3), 20–32, doi:10.1016/S0973-0826(08)60464-0, 2004.
- 487 Bond, T. C., Doherty, S. J., Fahey, D. W., Forster, P. M., Berntsen, T., Deangelo, B. J., Flanner,
488 M. G., Ghan, S., Kärcher, B., Koch, D., Kinne, S., Kondo, Y., Quinn, P. K., Sarofim, M. C.,
489 Schultz, M. G., Schulz, M., Venkataraman, C., Zhang, H., Zhang, S., Bellouin, N., Guttikunda,
490 S. K., Hopke, P. K., Jacobson, M. Z., Kaiser, J. W., Klimont, Z., Lohmann, U., Schwarz, J. P.,
491 Shindell, D., Storelvmo, T., Warren, S. G. and Zender, C. S.: Bounding the role of black carbon
492 in the climate system: A scientific assessment, J. Geophys. Res. Atmos., 118(11), 5380–5552,
493 doi:10.1002/jgrd.50171, 2013.



- 494 Bonjour, S., Wolf, J. and Lahiff, M.: Solid Fuel Use for Household Cooking : Country and
495 Regional Estimates for 1980 – 2010 Solid Fuel Use for Household Cooking : Country and
496 Regional Estimates, , 784(December 2014), 784–790, doi:10.1289/ehp.1205987, 2013.
- 497 Boucher, O., Randall, D., Artaxo, P., Bretherton, C., Feingold, G., Forster, P., Kerminen, V.-M.
498 V.-M., Kondo, Y., Liao, H., Lohmann, U., Rasch, P., Satheesh, S. K., Sherwood, S., Stevens, B.,
499 Zhang, X. Y. and Zhan, X. Y.: Clouds and Aerosols, Clim. Chang. 2013 Phys. Sci. Basis.
500 Contrib. Work. Gr. I to Fifth Assess. Rep. Intergov. Panel Clim. Chang., 571–657,
501 doi:10.1017/CBO9781107415324.016, 2013.
- 502 Butt, E. W., Rap, A., Schmidt, A., Scott, C. E., Pringle, K. J., Reddington, C. L., Richards, N. A.
503 D., Woodhouse, M. T., Ramirez-Villegas, J., Yang, H., Vakkari, V., Stone, E. A., Rupakheti, M.,
504 Praveen, P. S., Van Zyl, P. G., Beukes, J. P., Josipovic, M., Mitchell, E. J. S., Sallu, S. M.,
505 Forster, P. M. and Spracklen, D. V.: The impact of residential combustion emissions on
506 atmospheric aerosol, human health, and climate, Atmos. Chem. Phys., 16(2), 873–905,
507 doi:10.5194/acp-16-873-2016, 2016.
- 508 Carter, E., Archer-Nicholls, S., Ni, K., Lai, A. M., Niu, H., Secret, M. H., Sauer, S. M., Schauer,
509 J. J., Ezzati, M., Wiedinmyer, C., Yang, X. and Baumgartner, J.: Seasonal and Diurnal Air
510 Pollution from Residential Cooking and Space Heating in the Eastern Tibetan Plateau, Environ.
511 Sci. Technol., 50(15), 8353–8361, doi:10.1021/acs.est.6b00082, 2016.
- 512 Chow, J. C., Watson, J. G., Pritchett, L. C., Pierson, W. R., Frazer, C. A. and Purcell, R. G.: THE
513 DRI THERMAL/OPTICAL REFLECTANCE CARBON ANALYSIS SYSTEM :
514 DESCRIPTION, EVALUATION A N D APPLICATIONS IN U.S. AIR QUALITY STUDIES,
515 Atmos. Environ., 27A(8), 1185–1201, 1993.
- 516 Chow, J. C., Watson, J. G., Chen, L.-W. A., Arnott, W. P. and Moosmuller, H.: Equivalence of
517 Elemental Carbon by Thermal/Optical Reflectance and Transmittance with Different
518 Temperature Protocols, Environ. Sci. Technol., 38(16), 4414–4422, 2004.
- 519 Chung, S. H.: Climate response of direct radiative forcing of anthropogenic black carbon, J.
520 Geophys. Res., 110(D11), D11102, doi:10.1029/2004JD005441, 2005.



- 521 Chung, S. H. and Seinfeld, J. H.: Global distribution and climate forcing of carbonaceous
522 aerosols, *J. Geophys. Res. Atmos.*, 107(19), doi:10.1029/2001JD001397, 2002.
- 523 Chylek, P. and Wong, J.: Effect of absorbing aerosols on global radiation budget, *Geophys. Res.*
524 *Lett.*, 22(8), 929–931, 1995.
- 525 Cozic, J., Mertes, S., Verheggen, B., Cziczo, D. J., Gallavardin, S. J., Walter, S., Baltensperger,
526 U. and Weingartner, E.: Black carbon enrichment in atmospheric ice particle residuals observed
527 in lower tropospheric mixed phase clouds, *J. Geophys. Res. Atmos.*, 113(15), 1–11,
528 doi:10.1029/2007JD009266, 2008.
- 529 DeMott, P. J., Chen, Y., Kreidenweis, S. M., Rogers, D. C. and Sherman, D. E.: Ice formation by
530 black carbon particles, *Geophys. Res. Lett.*, 26(16), 2429–2432, doi:10.1029/1999GL900580,
531 1999.
- 532 Dubovikl, O. and King, M. D.: A flexible inversion algorithm for retrieval of aerosol optical
533 properties from Sun and sky radiance measurements, *J. Geophys. Res.*, 105696(27), 673–20,
534 doi:10.1029/2000JD900282, 2000.
- 535 EMEP/MSC-W, EMEP/CCC, EMEP/CEIP, IDAEA-CSIC, CCE/RIVM and FMI:
536 Transboundary particulate matter, photo-oxidants, acidifying and eutrophying components.,
537 2014.
- 538 Emmons, L. K., Walters, S., Hess, P. G., Lamarque, J.-F., Pfister, G. G., Fillmore, D., Granier,
539 C., Guenther, A., Kinnison, D., Laepple, T., Orlando, J., Tie, X., Tyndall, G., Wiedinmyer, C.,
540 Baughcum, S. L. and Kloster, S.: Description and evaluation of the Model for Ozone and Related
541 chemical Tracers, version 4 (MOZART-4), *Geosci. Model Dev.*, 3, 43–67, doi:10.5194/gmd-3-
542 43-2010, 2010.
- 543 Ezzati, M. and Kammen, D. M.: The health impacts of exposure to indoor air pollution from
544 solid fuels in developing countries: Knowledge, gaps, and data needs, *Environ. Health Perspect.*,
545 110(11), 1057–1068, doi:10.1289/ehp.021101057, 2002.
- 546 Fierce, L., Riemer, N. and Bond, T. C.: Toward reduced representation of mixing state for
547 simulating aerosol effects on climate, *Bull. Am. Meteorol. Soc.*, 98(5), 971–980,



- 548 doi:10.1175/BAMS-D-16-0028.1, 2017.
- 549 Flanner, M. G., Zender, C. S., Randerson, J. T. and Rasch, P. J.: Present-day climate forcing and
550 response from black carbon in snow, *J. Geophys. Res. Atmos.*, 112(11), 1–17,
551 doi:10.1029/2006JD008003, 2007.
- 552 Gadhavi, H. S., Renuka, K., Ravi Kiran, V., Jayaraman, A., Stohl, A., Klimont, Z. and Beig, G.:
553 Evaluation of black carbon emission inventories using a Lagrangian dispersion model - A case
554 study over southern India, *Atmos. Chem. Phys.*, 15(3), 1447–1461, doi:10.5194/acp-15-1447-
555 2015, 2015.
- 556 Garland, C., Delapena, S., Prasad, R., L'Orange, C., Alexander, D. and Johnson, M.: Black
557 carbon cookstove emissions: A field assessment of 19 stove/fuel combinations, *Atmos. Environ.*,
558 169, 140–149, doi:10.1016/j.atmosenv.2017.08.040, 2017.
- 559 GBD 2015 Risk Factors Collaborators: Global, regional, and national comparative risk
560 assessment of 79 behavioural, environmental and occupational, and metabolic risks or clusters of
561 risks, 1990–2015: a systematic analysis for the Global Burden of Disease Study 2015, *Lancet*,
562 388(10053), 1659–1724, doi:10.1016/S0140-6736(16)31679-8, 2016.
- 563 Gettelman, A., Liu, X., Barahona, D., Lohmann, U. and Chen, C.: Climate impacts of ice
564 nucleation, *J. Geophys. Res. Atmos.*, 117(20), 1–14, doi:10.1029/2012JD017950, 2012.
- 565 Ghan, S. J.: Technical note: Estimating aerosol effects on cloud radiative forcing, *Atmos. Chem.*
566 *Phys.*, 13(19), 9971–9974, doi:10.5194/acp-13-9971-2013, 2013.
- 567 Ghan, S. J., Liu, X., Easter, R. C., Zaveri, R., Rasch, P. J., Yoon, J. H. and Eaton, B.: Toward a
568 minimal representation of aerosols in climate models: Comparative decomposition of aerosol
569 direct, semidirect, and indirect radiative forcing, *J. Clim.*, 25(19), 6461–6476, doi:10.1175/JCLI-
570 D-11-00650.1, 2012.
- 571 He, C., Li, Q. B., Liou, K. N., Zhang, J., Qi, L., Mao, Y., Gao, M., Lu, Z., Streets, D. G., Zhang,
572 Q., Sarin, M. M. and Ram, K.: A global 3-D CTM evaluation of black carbon in the Tibetan
573 Plateau, *Atmos. Chem. Phys.*, 14(13), 7091–7112, doi:10.5194/acp-14-7091-2014, 2014.



- 574 He, J. and Zhang, Y.: Improvement and further development in CESM/CAM5: Gas-phase
575 chemistry and inorganic aerosol treatments, *Atmos. Chem. Phys.*, 14(17), 9171–9200,
576 doi:10.5194/acp-14-9171-2014, 2014.
- 577 Holben, B. N., Eck, T. F., Slutsker, I., Tanré, D., Buis, J. P., Setzer, A., Vermote, E., Reagan, J.
578 A., Kaufman, Y. J., Nakajima, T., Lavenu, F., Jankowiak, I. and Smirnov, A.: AERONET—A
579 Federated Instrument Network and Data Archive for Aerosol Characterization, *Remote Sens.*
580 *Environ.*, 66(1), 1–16, doi:10.1016/S0034-4257(98)00031-5, 1998.
- 581 Holben, B. N., Tanré, D., Smirnov, a., Eck, T. F., Slutsker, I., Abuhassan, N., Newcomb, W. W.,
582 Schafer, J. S., Chatenet, B., Lavenu, F., Kaufman, Y. J., Castle, J. Vande, Setzer, a., Markham,
583 B., Clark, D., Frouin, R., Halthore, R., Karneli, a., O'Neill, N. T., Pietras, C., Pinker, R. T.,
584 Voss, K. and Zibordi, G.: An emerging ground-based aerosol climatology: Aerosol optical depth
585 from AERONET, *J. Geophys. Res.*, 106(D11), 12067, doi:10.1029/2001JD900014, 2001.
- 586 Huang, Y., Wu, S., Dubey, M. K. and French, N. H. F.: Impact of aging mechanism on model
587 simulated carbonaceous aerosols, *Atmos. Chem. Phys.*, 13(13), 6329–6343, doi:10.5194/acp-13-
588 6329-2013, 2013.
- 589 Jacobson, M. Z.: Global direct radiative forcing due to multicomponent natural and anthropogenic
590 aerosols, *J. Geophys. Res.*, 106(D2), 1551–1568, doi:10.1029/2000JD900514, 2001a.
- 591 Jacobson, M. Z.: Strong radiative heating due to the mixing state of black carbon in atmospheric
592 aerosols., *Nature*, 409(6821), 695–697, doi:10.1038/35055518, 2001b.
- 593 Janssens-Maenhout, G., Crippa, M., Guizzardi, D., Dentener, F., Muntean, M., Pouliot, G.,
594 Keating, T., Zhang, Q., Kurokawa, J., Wankmüller, R., Denier van der Gon, H., Kuenen, J. J. P.,
595 Klimont, Z., Frost, G., Darras, S., Koffi, B. and Li, M.: HTAP_v2.2: a mosaic of regional and
596 global emission grid maps for 2008 and 2010 to study hemispheric transport of air pollution,
597 *Atmos. Chem. Phys.*, 15(19), 11411–11432, doi:10.5194/acp-15-11411-2015, 2015.
- 598 Karcher, B. and Hendricks, J.: Physically based parameterization of cirrus cloud formation for
599 use in global atmospheric models, *J. Geophys. Res.*, 111, D01205, doi:10.1029/2005JD006219,
600 2006.



- 601 Klimont, Z., Cofala, J., Wei, W., Zhang, C., Wang, S., Kejun, J., Bhandari, P., Mathur, R.,
602 Purohit, P., Rafaj, P., Chambers, A., Amann, M. and Hao, J.: Projections of SO₂, NO_x and
603 carbonaceous aerosols emissions in Asia, *Tellus, Ser. B Chem. Phys. Meteorol.*, (61B), 602–617,
604 doi:10.1111/j.1600-0889.2009.00428.x, 2009.
- 605 Klimont, Z., Kupiainen, K., Heyes, C., Purohit, P., Cofala, J., Rafaj, P., Borcken-Kleefeld, J. and
606 Schöpp, W.: Global anthropogenic emissions of particulate matter including black carbon,
607 *Atmos. Chem. Phys.*, 17(14), 8681–8723, doi:10.5194/acp-17-8681-2017, 2017.
- 608 Kodros, J. K., Scott, C. E., Farina, S. C., Lee, Y. H., L'Orange, C., Volckens, J. and Pierce, J. R.:
609 Uncertainties in global aerosols and climate effects due to biofuel emissions, *Atmos. Chem.*
610 *Phys.*, 15(15), 8577–8596, doi:10.5194/acp-15-8577-2015, 2015.
- 611 Koehler, K. A., DeMott, P. J., Kreidenweis, S. M., Popovicheva, O. B., Petters, M. D., Carrico,
612 C. M., Kireeva, E. D., Khokhlova, T. D. and Shonija, N. K.: Cloud condensation nuclei and ice
613 nucleation activity of hydrophobic and hydrophilic soot particles, *Phys. Chem. Chem. Phys.*,
614 11(36), 7906–7920, doi:10.1039/b916865f, 2009.
- 615 Kooperman, G. J., Pritchard, M. S., Ghan, S. J., Wang, M., Somerville, R. C. J. and Russell, L.
616 M.: Constraining the influence of natural variability to improve estimates of global aerosol
617 indirect effects in a nudged version of the Community Atmosphere Model 5, *J. Geophys. Res.*
618 *Atmos.*, 117(23), 1–16, doi:10.1029/2012JD018588, 2012.
- 619 Kulkarni, G., China, S., Liu, S., Nandasiri, M., Sharma, N., Wilson, J., Aiken, A. C., Chand, D.,
620 Laskin, A., Mazzoleni, C., Pekour, M., Shilling, J., Shutthanandan, V., Zelenyuk, A. and Zaveri,
621 R. A.: Ice nucleation activity of diesel soot particles at cirrus relevant temperature conditions:
622 Effects of hydration, secondary organics coating, soot morphology, and coagulation, *Geophys.*
623 *Res. Lett.*, 43(7), 3580–3588, doi:10.1002/2016GL068707, 2016.
- 624 Lacey, F. and Henze, D.: Global climate impacts of country-level primary carbonaceous aerosol
625 from solid-fuel cookstove emissions, *Environ. Res. Lett.*, 10(11), 114003, doi:10.1088/1748-
626 9326/10/11/114003, 2015.
- 627 Lacey, F. G., Henze, D. K., Lee, C. J., van Donkelaar, A. and Martin, R. V.: Transient climate



- 628 and ambient health impacts due to national solid fuel cookstove emissions, *Proc. Natl. Acad.*
629 *Sci.*, 114(6), 1269–1274, doi:10.1073/pnas.1612430114, 2017.
- 630 Lamarque, J. F., Emmons, L. K., Hess, P. G., Kinnison, D. E., Tilmes, S., Vitt, F., Heald, C. L.,
631 Holland, E. A., Lauritzen, P. H., Neu, J., Orlando, J. J., Rasch, P. J. and Tyndall, G. K.: CAM-
632 chem: Description and evaluation of interactive atmospheric chemistry in the Community Earth
633 System Model, *Geosci. Model Dev.*, 5(2), 369–411, doi:10.5194/gmd-5-369-2012, 2012.
- 634 Legros, G., Havet, I., Bruce, N. and Bonjour, S.: The Energy Access Situation in Developing
635 Countries, WHO UNDP, 142 [online] Available from:
636 <http://scholar.google.com/scholar?hl=en&btnG=Search&q=intitle:THE+ENERGY+ACCESS+SITUATION+IN+DEVELOPING+COUNTRIES+A+Review+Focusing+on+the#0>, 2009.
637
- 638 Lelieveld, J., Evans, J. S., Fnais, M., Giannadaki, D. and Pozzer, A.: The contribution of outdoor
639 air pollution sources to premature mortality on a global scale, *Nature*, 525(7569), 367–371,
640 doi:10.1038/nature15371, 2015.
- 641 Liu, J., Mauzerall, D. L., Chen, Q., Zhang, Q., Song, Y., Peng, W., Klimont, Z., Qiu, X., Zhang,
642 S., Hu, M., Lin, W., Smith, K. R. and Zhu, T.: Air pollutant emissions from Chinese households:
643 A major and underappreciated ambient pollution source, *Proc. Natl. Acad. Sci.*, 113(28), 7756–
644 7761, doi:10.1073/pnas.1604537113, 2016.
- 645 Liu, X. and Penner, J. E.: Ice nucleation parameterization for global models, *Meteorol.*
646 *Zeitschrift*, 14(4), 499–514, doi:10.1127/0941-2948/2005/0059, 2005.
- 647 Liu, X., Easter, R. C., Ghan, S. J., Zaveri, R., Rasch, P., Shi, X., Lamarque, J. F., Gettelman, A.,
648 Morrison, H., Vitt, F., Conley, A., Park, S., Neale, R., Hannay, C., Ekman, A. M. L., Hess, P.,
649 Mahowald, N., Collins, W., Iacono, M. J., Bretherton, C. S., Flanner, M. G. and Mitchell, D.:
650 Toward a minimal representation of aerosols in climate models: Description and evaluation in
651 the Community Atmosphere Model CAM5, *Geosci. Model Dev.*, 5(3), 709–739,
652 doi:10.5194/gmd-5-709-2012, 2012.
- 653 Lohmann, U.: A glaciation indirect aerosol effect caused by soot aerosols, *Geophys. Res. Lett.*,
654 29(4), 1052, doi:10.1029/2001gl014357, 2002.



- 655 Lohmann, U., Feichter, J., Penner, J. and Leaitch, R.: Indirect effect of sulfate and carbonaceous
656 aerosols: A mechanistic treatment, *J. Geophys. Res. Atmos.*, 105(D10), 12193–12206,
657 doi:10.1029/1999JD901199, 2000.
- 658 Lu, Z., Zhang, Q. and Streets, D. G.: Sulfur dioxide and primary carbonaceous aerosol emissions
659 in China and India, 1996–2010, *Atmos. Chem. Phys.*, 11(18), 9839–9864, doi:10.5194/acp-11-
660 9839-2011, 2011.
- 661 Malm, W. C., Sisler, J. F., Huffman, D., Eldred, R. A. and Cahill, T. A.: Spatial and seasonal
662 trends in particle concentration and optical extinction in the United States, *J. Geophys. Res.*,
663 99(D1), 1347–1370, doi:10.1029/93JD02916, 1994.
- 664 Myhre, G., Samset, B. H., Schulz, M., Balkanski, Y., Bauer, S., Berntsen, T. K., Bian, H.,
665 Bellouin, N., Chin, M., Diehl, T., Easter, R. C., Feichter, J., Ghan, S. J., Hauglustaine, D.,
666 Iversen, T., Kinne, S., Kirkevåg, A., Lamarque, J. F., Lin, G., Liu, X., Lund, M. T., Luo, G., Ma,
667 X., Van Noije, T., Penner, J. E., Rasch, P. J., Ruiz, A., Seland, Skeie, R. B., Stier, P., Takemura,
668 T., Tsigaridis, K., Wang, P., Wang, Z., Xu, L., Yu, H., Yu, F., Yoon, J. H., Zhang, K., Zhang, H.
669 and Zhou, C.: Radiative forcing of the direct aerosol effect from AeroCom Phase II simulations,
670 *Atmos. Chem. Phys.*, 13(4), 1853–1877, doi:10.5194/acp-13-1853-2013, 2013.
- 671 Penner, J. E., Dickinson, R. E. and O'Neill, C. A.: Effects of Aerosol from Biomass Burning on
672 the Global Radiation Budget, *Science* (80-.), 256(June), 1432–1435, 1992.
- 673 Penner, J. E., Chen, Y., Wang, M. and Liu, X.: Possible influence of anthropogenic aerosols on
674 cirrus clouds and anthropogenic forcing, *Atmos. Chem. Phys.*, 9(3), 879–896, doi:10.5194/acp-9-
675 879-2009, 2009.
- 676 Pierce, J. R., Chen, K. and Adams, P. J.: Contribution of carbonaceous aerosol to cloud
677 condensation nuclei: processes and uncertainties evaluated with a global aerosol microphysics
678 model, *Atmos. Chem. Phys. Discuss.*, 7(3), 7723–7765, doi:10.5194/acpd-7-7723-2007, 2007.
- 679 Quennehen, B., Raut, J. C., Law, K. S., Daskalakis, N., Ancellet, G., Clerbaux, C., Kim, S. W.,
680 Lund, M. T., Myhre, G., Olivie, D. J. L., Safieddine, S., Skeie, R. B., Thomas, J. L., Tsyro, S.,
681 Bazureau, A., Bellouin, N., Hu, M., Kanakidou, M., Klimont, Z., Kupiainen, K.,



- 682 Myriokefalitakis, S., Quaas, J., Rumbold, S. T., Schulz, M., Cherian, R., Shimizu, A., Wang, J.,
683 Yoon, S. C. and Zhu, T.: Multi-model evaluation of short-lived pollutant distributions over east
684 Asia during summer 2008, *Atmos. Chem. Phys.*, 16(17), 10765–10792, doi:10.5194/acp-16-
685 10765-2016, 2016.
- 686 Reddington, C. L., Spracklen, D. V., Artaxo, P., Ridley, D. A., Rizzo, L. V. and Arana, A.:
687 Analysis of particulate emissions from tropical biomass burning using a global aerosol model
688 and long-term surface observations, *Atmos. Chem. Phys.*, 16(17), 11083–11106,
689 doi:10.5194/acp-16-11083-2016, 2016.
- 690 Riahi, K., Rao, S., Krey, V., Cho, C., Chirkov, V., Fischer, G., Kindermann, G., Nakicenovic, N.
691 and Rafaj, P.: RCP 8.5-A scenario of comparatively high greenhouse gas emissions, *Clim.*
692 *Change*, 109(1), 33–57, doi:10.1007/s10584-011-0149-y, 2011.
- 693 Schulz, M., Textor, C., Kinne, S., Balkanski, Y., Bauer, S., Berntsen, T., Berglen, T., Boucher,
694 O., Dentener, F., Guibert, S., Isaksen, I. S. a., Iversen, T., Koch, D., Kirkevåg, A., Liu, X.,
695 Montanaro, V., Myhre, G., Penner, J. E., Pitari, G., Reddy, S., Seland, Ø., Stier, P. and
696 Takemura, T.: Radiative forcing by aerosols as derived from the AeroCom present-day and pre-
697 industrial simulations, *Atmos. Chem. Phys.*, 6, 5225–5246, doi:10.5194/acpd-6-5095-2006,
698 2006.
- 699 Smith, K. R., Bruce, N., Balakrishnan, K., Adair-Rohani, H., Balmes, J., Chafe, Z., Dherani, M.,
700 Hosgood, H. D., Mehta, S., Pope, D. and Rehfuess, E.: Millions Dead: How Do We Know and
701 What Does It Mean? Methods Used in the Comparative Risk Assessment of Household Air
702 Pollution, *Annu. Rev. Public Health*, 35(1), 185–206, doi:10.1146/annurev-publhealth-032013-
703 182356, 2014.
- 704 Spracklen, D. V., Jimenez, J. L., Carslaw, K. S., Worsnop, D. R., Evans, M. J., Mann, G. W.,
705 Zhang, Q., Canagaratna, M. R., Allan, J., Coe, H., McFiggans, G., Rap, A. and Forster, P.:
706 Aerosol mass spectrometer constraint on the global secondary organic aerosol budget, *Atmos.*
707 *Chem. Phys.*, 11(23), 12109–12136, doi:10.5194/acp-11-12109-2011, 2011a.
- 708 Spracklen, D. V., Carslaw, K. S., Pöschl, U., Rap, A. and Forster, P. M.: Global cloud
709 condensation nuclei influenced by carbonaceous combustion aerosol, *Atmos. Chem. Phys.*,



- 710 11(17), 9067–9087, doi:10.5194/acp-11-9067-2011, 2011b.
- 711 Stohl, A., Aamaas, B., Amann, M., Baker, L. H., Bellouin, N., Berntsen, T. K., Boucher, O.,
712 Cherian, R., Collins, W., Daskalakis, N., Dusinska, M., Eckhardt, S., Fuglestvedt, J. S., Harju,
713 M., Heyes, C., Hodnebrog, Hao, J., Im, U., Kanakidou, M., Klimont, Z., Kupiainen, K., Law, K.
714 S., Lund, M. T., Maas, R., MacIntosh, C. R., Myhre, G., Myriokefalitakis, S., Olivie, D., Quaas,
715 J., Quennehen, B., Raut, J. C., Rumbold, S. T., Samset, B. H., Schulz, M., Seland, Shine, K. P.,
716 Skeie, R. B., Wang, S., Yttri, K. E. and Zhu, T.: Evaluating the climate and air quality impacts of
717 short-lived pollutants, *Atmos. Chem. Phys.*, 15(18), 10529–10566, doi:10.5194/acp-15-10529-
718 2015, 2015.
- 719 Streets, D. G., Yan, F., Chin, M., Diehl, T., Mahowald, N., Schultz, M., Wild, M., Wu, Y. and
720 Yu, C.: Anthropogenic and natural contributions to regional trends in aerosol optical depth,
721 1980–2006, *J. Geophys. Res. Atmos.*, 114(14), 1–16, doi:10.1029/2008JD011624, 2009.
- 722 Textor, C., Schulz, M., Guibert, S., Kinne, S., Balkanski, Y., Bauer, S., Berntsen, T., Berglen, T.,
723 Boucher, O., Chin, M., Dentener, F., Diehl, T., Easter, R., Feichter, H., Fillmore, D., Ghan, S.,
724 Ginoux, P., Gong, S., Grini, A., Hendricks, J., Horowitz, L., Huang, P., Isaksen, I., Iversen, I.,
725 Kloster, S., Koch, D., Kirkevåg, A., Kristjansson, J. E., Krol, M., Lauer, A., Lamarque, J. F., Liu,
726 X., Montanaro, V., Myhre, G., Penner, J., Pitari, G., Reddy, S., Seland, Ø., Stier, P., Takemura,
727 T. and Tie, X.: Analysis and quantification of the diversities of aerosol life cycles within
728 AeroCom, *Atmos. Chem. Phys.*, 6(7), 1777–1813, doi:10.5194/acp-6-1777-2006, 2006.
- 729 Tilmes, S., Lamarque, J. F., Emmons, L. K., Kinnison, D. E., Ma, P. L., Liu, X., Ghan, S.,
730 Bardeen, C., Arnold, S., Deeter, M., Vitt, F., Ryerson, T., Elkins, J. W., Moore, F., Spackman, J.
731 R. and Val Martin, M.: Description and evaluation of tropospheric chemistry and aerosols in the
732 Community Earth System Model (CESM1.2), *Geosci. Model Dev.*, 8(5), 1395–1426,
733 doi:10.5194/gmd-8-1395-2015, 2015.
- 734 Venkataraman, C.: Residential Biofuels in South Asia: Carbonaceous Aerosol Emissions and
735 Climate Impacts, *Science (80-.)*, 307(5714), 1454–1456, doi:10.1126/science.1104359, 2005.
- 736 Wang, Q., Jacob, D. J., Fisher, J. A., Mao, J., Leibensperger, E. M., Carouge, C. C., Le Sager, P.,
737 Kondo, Y., Jimenez, J. L., Cubison, M. J. and Doherty, S. J.: Sources of carbonaceous aerosols



- 738 and deposited black carbon in the Arctic in winter-spring: Implications for radiative forcing,
739 Atmos. Chem. Phys., 11(23), 12453–12473, doi:10.5194/acp-11-12453-2011, 2011.
- 740 Wang, Q., Jacob, D. J., Spackman, J. R., Perring, A. E., Schwarz, J. P., Moteki, N., Marais, E.
741 A., Ge, C., Wang, J. and Barrett, S. R. H.: Global budget and radiative forcing of black carbon
742 aerosol: Constraints from pole-to-pole (HIPPO) observations across the Pacific, J. Geophys.
743 Res., 119(1), 195–206, doi:10.1002/2013JD020824, 2014a.
- 744 Wang, X., Heald, C. L., Ridley, D. A., Schwarz, J. P., Spackman, J. R., Perring, A. E., Coe, H.,
745 Liu, D. and Clarke, A. D.: Exploiting simultaneous observational constraints on mass and
746 absorption to estimate the global direct radiative forcing of black carbon and brown carbon,
747 Atmos. Chem. Phys., 14(20), 10989–11010, doi:10.5194/acp-14-10989-2014, 2014b.
- 748 Zhang, L., Henze, D. K., Grell, G. A., Carmichael, G. R., Bousserez, N., Zhang, Q., Torres, O.,
749 Ahn, C., Lu, Z., Cao, J. and Mao, Y.: Constraining black carbon aerosol over Asia using OMI
750 aerosol absorption optical depth and the adjoint of GEOS-Chem, Atmos. Chem. Phys., 15(18),
751 10281–10308, doi:10.5194/acp-15-10281-2015, 2015.
- 752 Zhang, Q., Jimenez, J. L., Canagaratna, M. R., Allan, J. D., Coe, H., Ulbrich, I., Alfarra, M. R.,
753 Takami, A., Middlebrook, A. M., Sun, Y. L., Dzepina, K., Dunlea, E., Docherty, K., DeCarlo, P.
754 F., Salcedo, D., Onasch, T., Jayne, J. T., Miyoshi, T., Shimono, A., Hatakeyama, S., Takegawa,
755 N., Kondo, Y., Schneider, J., Drewnick, F., Borrmann, S., Weimer, S., Demerjian, K., Williams,
756 P., Bower, K., Bahreini, R., Cottrell, L., Griffin, R. J., Rautiainen, J., Sun, J. Y., Zhang, Y. M.
757 and Worsnop, D. R.: Ubiquity and dominance of oxygenated species in organic aerosols in
758 anthropogenically-influenced Northern Hemisphere midlatitudes, Geophys. Res. Lett., 34(13), 1–
759 6, doi:10.1029/2007GL029979, 2007.
- 760 Zheng, Y., Unger, N., Hodzic, A., Emmons, L., Knote, C., Tilmes, S., Lamarque, J. F. and Yu,
761 P.: Limited effect of anthropogenic nitrogen oxides on Secondary Organic Aerosol formation,
762 Atmos. Chem. Phys., 15(23), 23231–23277, doi:10.5194/acpd-15-23231-2015, 2015.
- 763
- 764



765 **Table 1. Annual budget for various species for the BASE, GBLSF_OFF and INDSF_OFF**
766 **simulations for the year 2010.**

| Specie | ECLIPSE V5a (BASE) ^a | GBLSF_OFF ^a | INDSF_OFF ^a |
|-----------------|---------------------------------|------------------------|------------------------|
| BC | 7.23 | 4.92 | 6.87 |
| POM | 18.9 | 8.53 | 17.2 |
| SO ₂ | 98.5 | 97.1 | 98.37 |
| NO _x | 120.5 | 118 | 119.8 |
| VOC | 81.1 | 52.4 | 76.6 |
| CO | 548 | 358 | 516 |
| NH ₃ | 54.9 | 54.6 | 54.87 |

767 ^aUnits are Tg specie/yr.

768

769

770

771

772

773

774

775

776

777



778 **Table 2. Model experiments setup.**

| Experiments | Anthropogenic emission scenario |
|-------------|---|
| BASE | ECLIPSE V5a |
| GBLSF_OFF | ECLIPSE V5a excluding global solid fuel cookstove emissions |
| INDSF_OFF | ECLIPSE V5a excluding Indian solid fuel cookstove emissions |

779

780

781

782

783

784

785

786

787

788

789

790

791

792



793 **Table 3. Global budgets, burden and lifetime of BC and POM from model control**
794 **simulations.**

| Specie | BC | POM |
|-----------------------------------|------|------|
| Sources (Tg specie/yr) | 9.73 | 49.9 |
| fossil fuel and biofuel emissions | 7.23 | 18.9 |
| biomass burning emissions | 2.5 | 31 |
| Sinks (Tg specie/yr) | 9.72 | 49.8 |
| Dry Deposition | 1.8 | 8.14 |
| Wet Deposition | 7.92 | 41.7 |
| Burden (Tg) | 0.12 | 0.66 |
| Lifetime (days) | 4.5 | 4.8 |

795

796

797

798

799

800

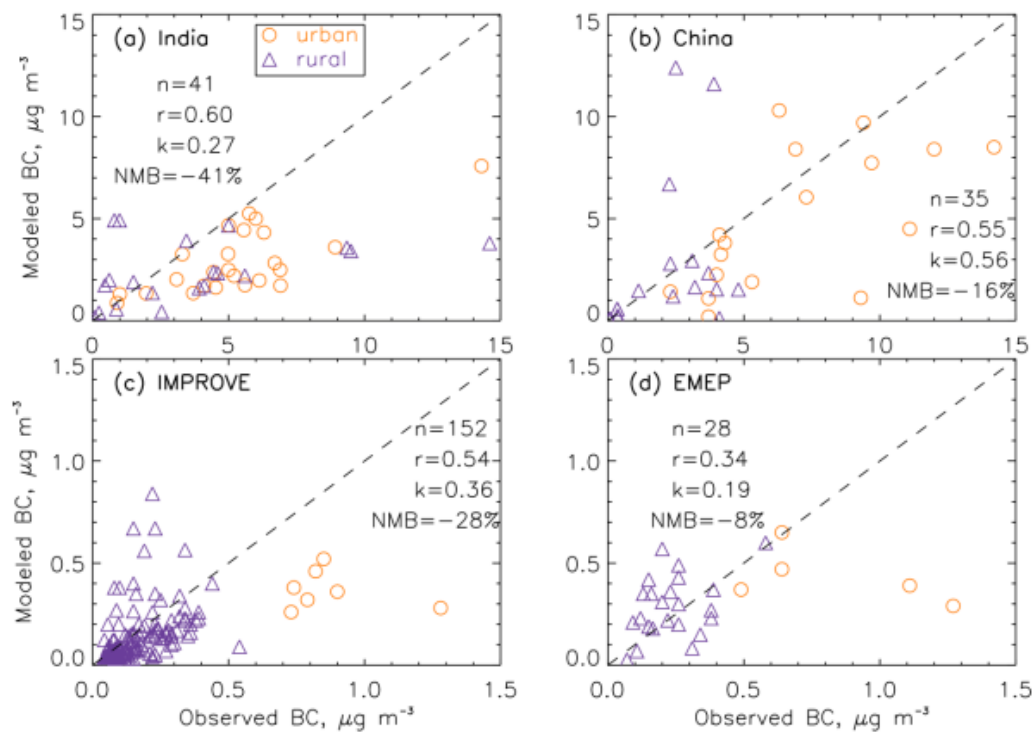
801

802

803

804

805



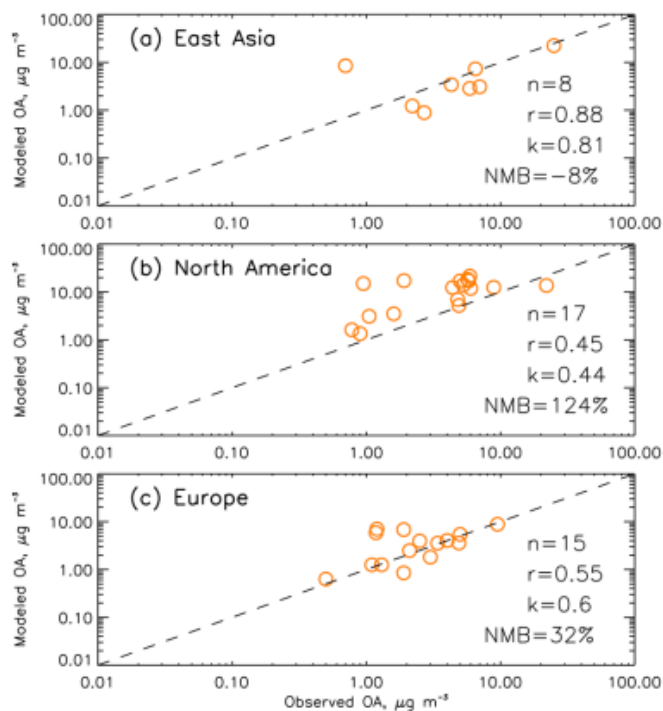
806

807 **Figure 1.** Comparisons of observational and model simulated annual mean surface BC
808 concentrations from (a) India, (b) China, (3) IMPROVE, and (d) EMEP. Urban and rural sites are
809 shown in orange circles and blue triangles for each region. For each panel, the total number of
810 observational sites (n), model-to-observation regression slopes (k), correlation coefficient (r) and
811 NMB values are included. The dashed line in each panel represents the 1:1 ratio.

812

813

814

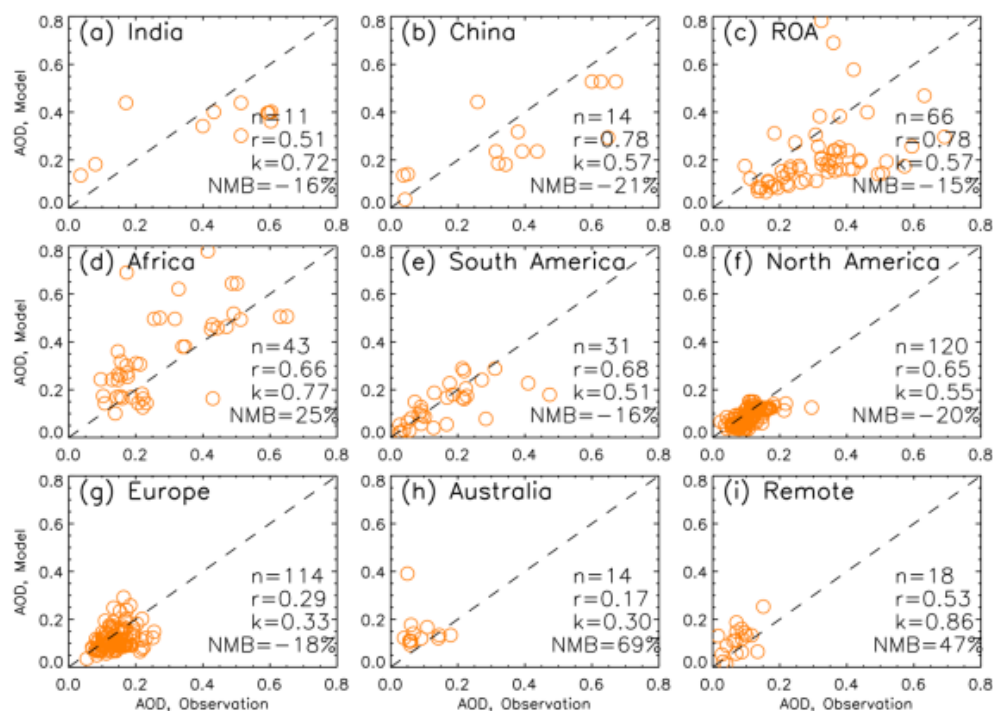


815

816 **Figure 2.** Comparisons of observational and model simulated surface OA concentrations from (a)
817 East Asia, (b) North America, and (c) Europe. For each panel, the total number of observational
818 sites (n), model-to-observation regression slopes (k), correlation coefficient (r) and NMB values
819 are included. The dashed line in each panel represents the 1:1 ratio.

820

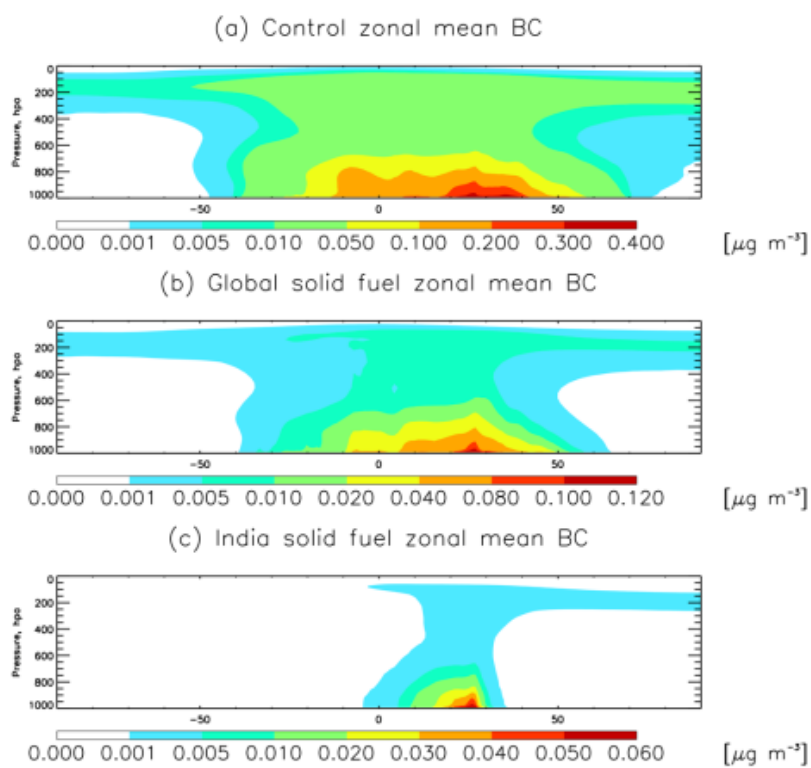
821



822

823 **Figure 3.** Scatter plots of AOD between model simulation and observations over (a) India, (b)
824 China, (c) Rest of Asia (ROA), excluding China and India, (d) Africa, (e) South America, (f) North
825 America, (g) Europe, (h) Australia and (i) Remote. For each panel, the total number of
826 observational sites (n), model-to-observation regression slopes (k), correlation coefficient (r) and
827 NMB are included.

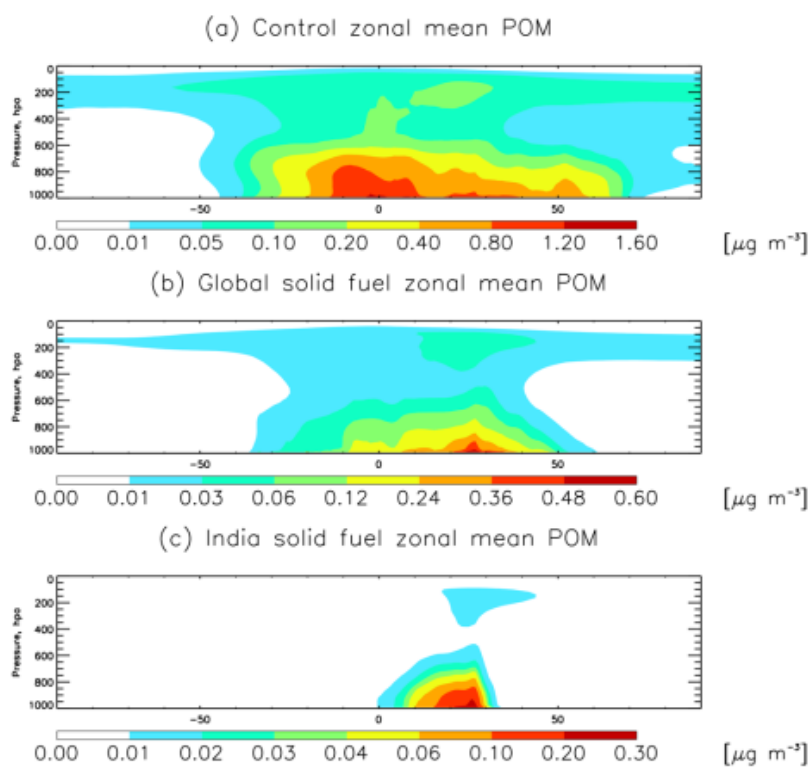
828



829

830 **Figure 4.** Annual zonal mean BC concentrations from (a) the BASE simulation, (b) the global and
831 (c) India solid fuel cookstove emissions.

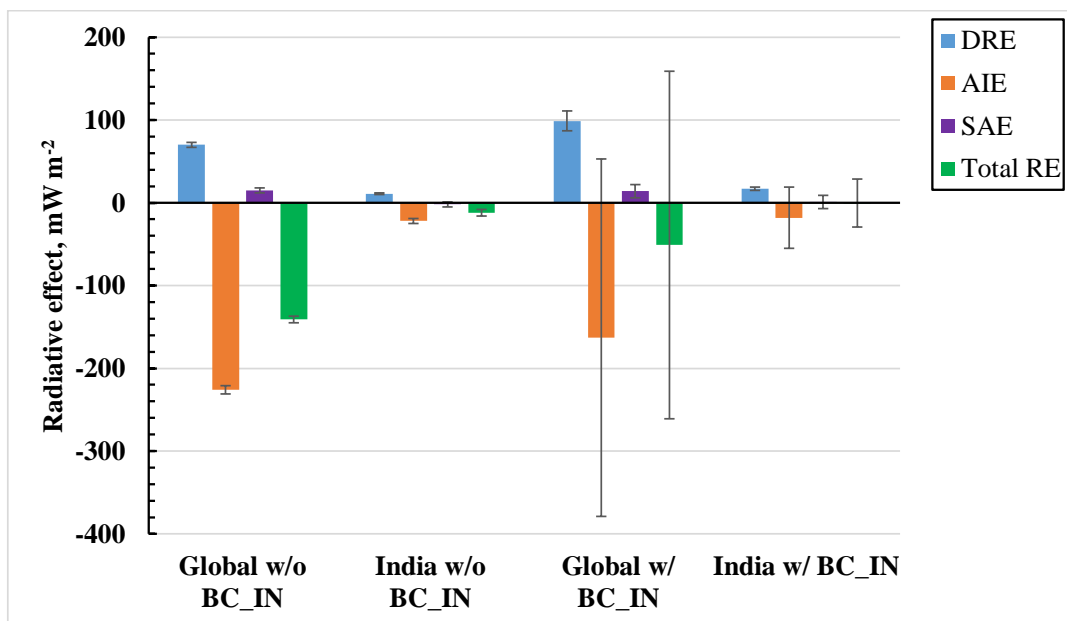
832



833

834 **Figure 5.** Same as Fig. 4 but for POM.

835



836

837 **Figure 6.** Radiative effect (RE) for global and Indian solid fuel cookstove aerosol emissions with
838 BC not serving as IN (w/o BC_IN) and BC as IN (BC_IN), with DRE (blue), AIE (orange), SAE
839 (purple) and total RE (green). Error bars represent one standard deviation for each RE. For BC as
840 IN, standard deviations of RE are solely based on the choices of maximum freezing efficiency of
841 BC as 0.01, 0.05 and 0.1 respectively.

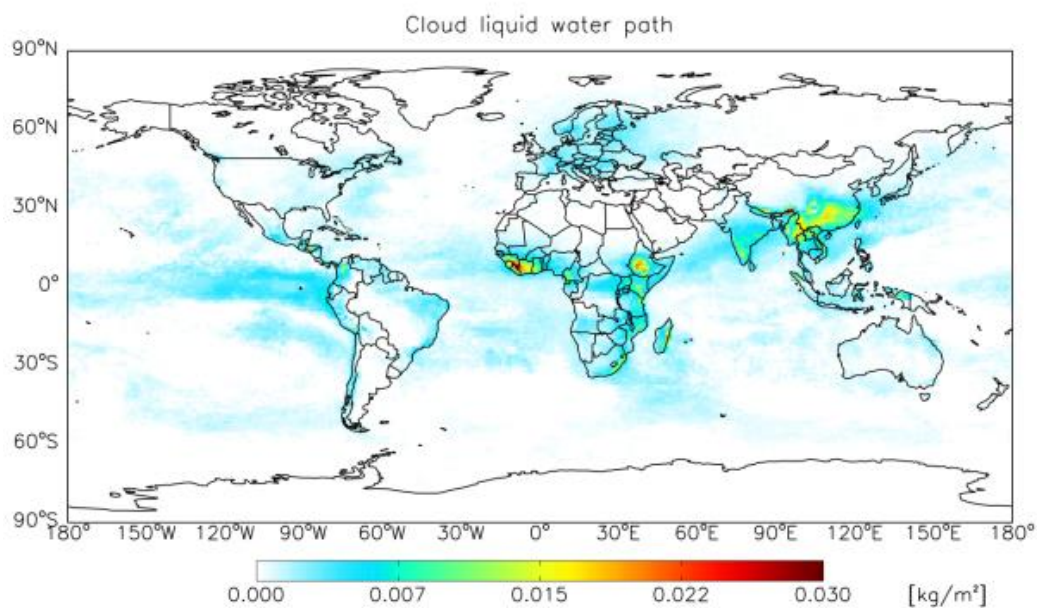
842

843

844

845

846



847

848 **Figure 7.** Global vertically-integrated cloud liquid water path from the global solid fuel cookstove
849 emissions.

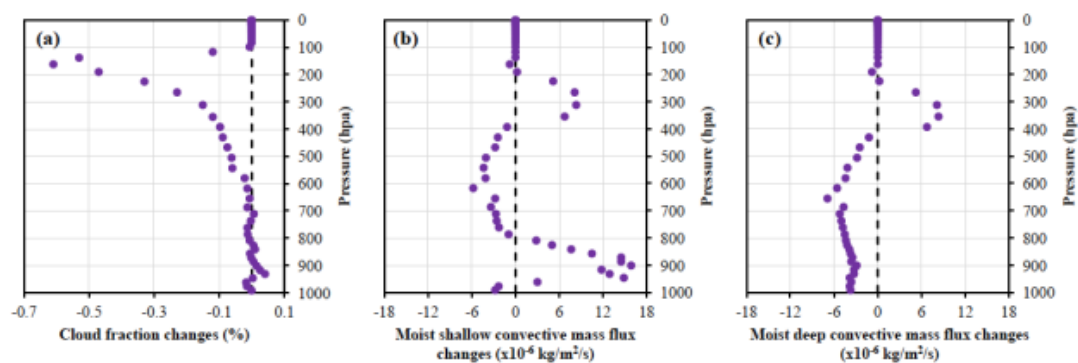
850

851

852

853

854



855

856 **Figure 8.** Changes in vertical cloud fractions (a), shallow (b) and deep (c) convective mass flux
857 within the India and Indian Ocean domain from global solid fuel cookstove emissions.

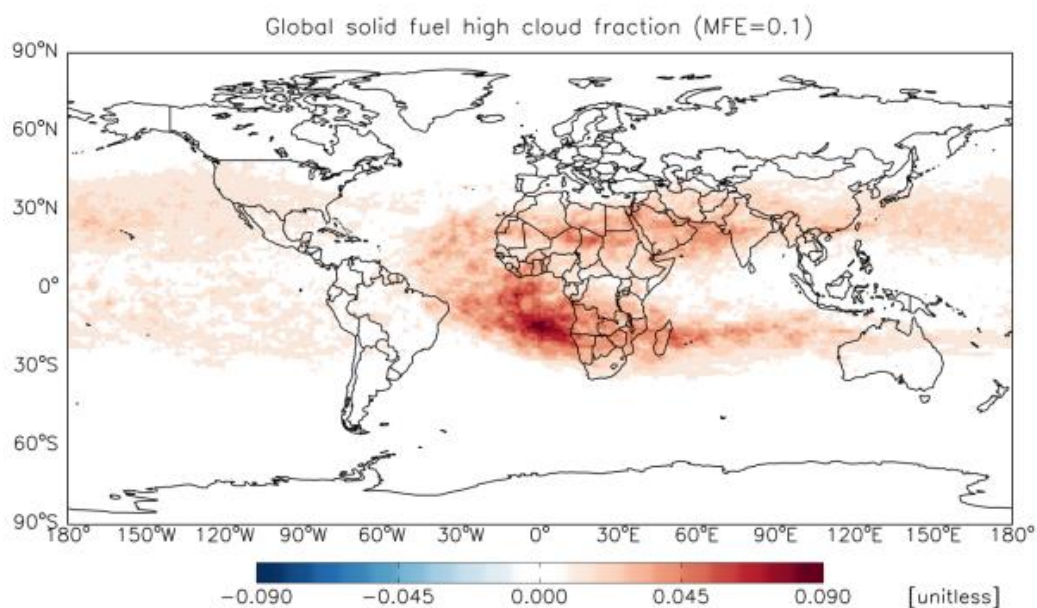
858

859

860

861

862



863

864 **Figure 9.** Global distribution of high cloud fraction due to solid fuel cookstove aerosol emissions
865 with BC as IN and MFE=0.1.

866

867

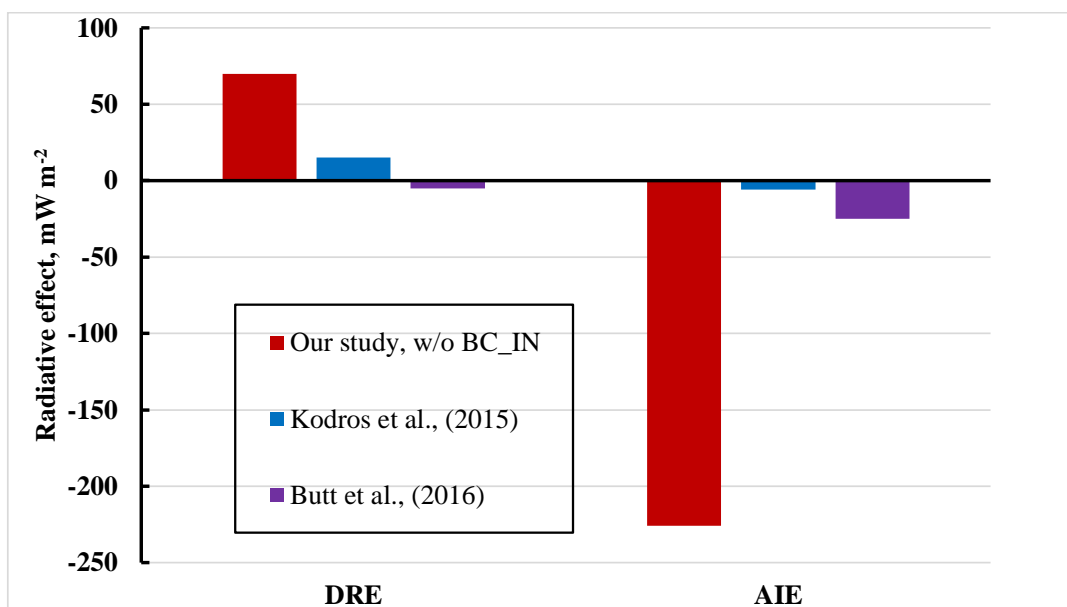
868

869

870

871

872



873

874

875 **Figure 10.** Comparisons of DRE (left) and AIE (right) radiative effects from global solid fuel
876 cookstove emissions in our control simulation with Kodros et al. (2015) and Butt et al. (2016).

877

878